Int. J. Microgravity Sci. Appl., **34** (3) (2017) 340305
DOI: 10.15011//jasma.34.340305

IIIII AMS2016 Proceedings IIIII
(Review)

# Emissivity Measurements of Molten Metals with an Electrostatic Levitator

Takehiko ISHIKAWA[1,2], Junpei T. OKADA[3], Paul-François PARADIS[4] and Yuki WATANABE[5]

**Abstract**

Spectral emissivity and constant heat capacities of molten metals (nickel, zirconium, rhodium, and niobium) at their melting temperatures were measured using containerless techniques. Samples were levitated in an electrostatic levitator and the radiation intensities from the molten samples were measured with spectrometers over a wide wavelength range. The spectrometers were calibrated with a blackbody radiation furnace and the spectral hemispherical emissivity was calculated. Then, the total hemispherical emissivity ($\varepsilon_T$) was obtained by integrating the spectral emissivity over wavelength. Finally, constant pressure heat capacity was calculated using the data obtained from the cooling curve and $\varepsilon_T$.

**Keyword(s):** Emissivity, High temperature melt, Levitation
Received: 14 December 2016, Accepted 30 May 2017, Published 31 July 2017

## 1. Introduction

To improve the accuracy of computer simulations for material processing such as casting and crystal growth, the knowledge of thermophysical properties of high temperature metals and alloys is paramount [1)]. Due to their high melting temperature and the risk of chemical reactions between samples and crucibles, property measurements of high temperature melts are very difficult with conventional methods.

In the recent decade, the electrostatic levitation method (ESL) [2)] has demonstrated a great potential to determine thermophysical properties of high temperature melts. In this method, the sample levitated by electrostatic forces under vacuum is isolated from any contact with a crucible or a substrate and from the contamination from a surrounding gas. Coupled with laser heating, the ESL has enabled accurate non-contact measurements of such thermophysical properties as density [3)], surface tension, and viscosity [4)] for several refractory metals.

Knowledge of the constant pressure heat capacity ($C_p$) and the emissivity ($\varepsilon$) is also important from both fundamental and industrial research standpoints. $C_p$ is needed to calculate thermodynamic state functions such as enthalpy, entropy, and Gibbs free energy. $\varepsilon$ is related to the index of refraction and extinction coefficient, and gives some insights about the structural properties. It is also important for accurate pyrometric temperature measurements. The total hemispherical emissivity ($\varepsilon_T$), which is the average value of emissivity in wavelength and in direction, is commonly used to calculate radiative heat transfer. Since these properties are difficult to measure for high temperature melts by conventional methods, levitation and pulse heating techniques were implemented and are now commonly used. Wunderlich [5)] and Kobatake [6)] used AC calorimetry methods combined with the electromagnetic levitator to measure the $C_p$ of molten zirconium alloys and silicon.

The ESL was also used and the ratios of constant pressure heat capacity over the total hemispherical emissivity ($C_p/\varepsilon_T$) for several refractory metals were obtained [7–10)]. However, independent measurements or knowledge of $\varepsilon_T$ is necessary to get $C_p$. Therefore, all the $C_p$ or $\varepsilon_T$ values obtained with electrostatic levitators were found by borrowing some of the literature values, either $\varepsilon_T$, $C_p$, or heat of fusion.

In this study, two spectrometers were combined with an electrostatic levitator to measure the spectral hemispherical emissivity of the levitated molten sample over a wide spectral range. Then, $\varepsilon_T$ was calculated by integrating the spectral hemispherical emissivity so that the $C_p$ of the molten sample could be obtained independently, without borrowing $\varepsilon_T$ from the literature. This paper details the experimental setup, explains the measurement method, and briefly summarizes the results for molten nickel, zirconium, niobium, and rhodium.

## 2. Experimental Setup

### 2.1 Electrostatic Levitator

The electrostatic levitation system used in our laboratory is similar to the one developed by Rhim *et al.* [2)] but includes

1 Japan Aerospace Exploration Agency, 2-1-1 Sengen, Tsukuba, Ibaraki, 305-8505, Japan.
2 SOKENDAI (The Graduate University for Advanced Studies), 3-1-1 Yoshinodai, Chuo-Ku, Sagamihara, 252-5210, Japan.
3 Tohoku University, 2-1-1 Katahira, Aoba-Ku, Sendai, 980-8577, Japan.
4 INO, 2740 Einstein St. Québec, Québec, G1P 4S4, Canada.
5 Advanced Engineering Services Co. Ltd., 1-6-1 Takezono, Tsukuba, Ibaraki, 305-0032, Japan.
(E-mail: Corresponding.ishikawa.takehiko@jaxa.jp)

 

several modifications. A detailed description of the facility is given elsewhere [10]. It consisted of a stainless-steel chamber that was evacuated to a pressure of around 5 x $10^{-5}$ Pa. The chamber housed a pair of parallel disk electrodes, typically 10 mm apart between which a positively charged sample was levitated. These electrodes were utilized to control the vertical position (z) of the specimen, which has a typical diameter of about 2 mm. In order to levitate the sample against gravity, a huge electric field of around 10 to 20 kV/cm was applied between the top and the bottom electrode. In addition, four spherical electrodes distributed around the bottom electrode were used for horizontal control (*x* and *y*). The lower electrode was surrounded by four coils that generated a rotating magnetic field which was used to control sample rotation [11]. The levitated sample was illuminated by red (645 nm) and green (532 nm) lasers for position sensing so that the high speed feedback control scheme could maintain the sample at a fixed and stable position.

Sample heating was achieved using $CO_2$ lasers (10.6 μm wavelength, total of 200 W), whose beams hit the sample from three directions separated by 120 degrees from each other in a horizontal plane. This multiple beam configuration minimized the laser induced disturbances (200 μm along the vertical axis and 100 μm along the horizontal axis) and increased the temperature homogeneity of the sample. The sample temperature data were obtained using a single-color pyrometer whose observation wavelength was 900 nm (with 200 nm full width at half maximum).

An observation camera, equipped with a telephoto objective in conjunction with a background UV (385 nm) lamp, provided a magnified view of the sample allowing the measurement of its radius.

## 2.2 Emissivity Measurement System

**Figure 1** illustrates the emissivity measurement system. The setup consisted of a multichannel photo spectrometer (Otsuka Electronics Co. Ltd. MCPD-3000), which covered the wavelengths ranging from 700 nm to 1000 nm, a FTIR (Newport Co. 80251) that covered a spectral interval from 1.1 to 6 μm, and a blackbody furnace (BBF) (MIKRON M335) which can reach a temperature as high as 1773 K. The measurement concept is to measure the spectral intensity of the radiation from the levitated sample and compare it with that of a blackbody to calculate the spectral emissivity. This technique is widely used and was recently implemented in conjunction with other containerless method that includes cold crucible [12], electromagnetic levitation [13], and electrostatic levitation [14].

Since the electrostatically levitated sample was smaller than that used with either the electromagnetic or the cold crucible, the radiation intensity from the sample was also smaller. In order to get a good signal to noise ratio, the measurement system should be as simple as possible to eliminate error

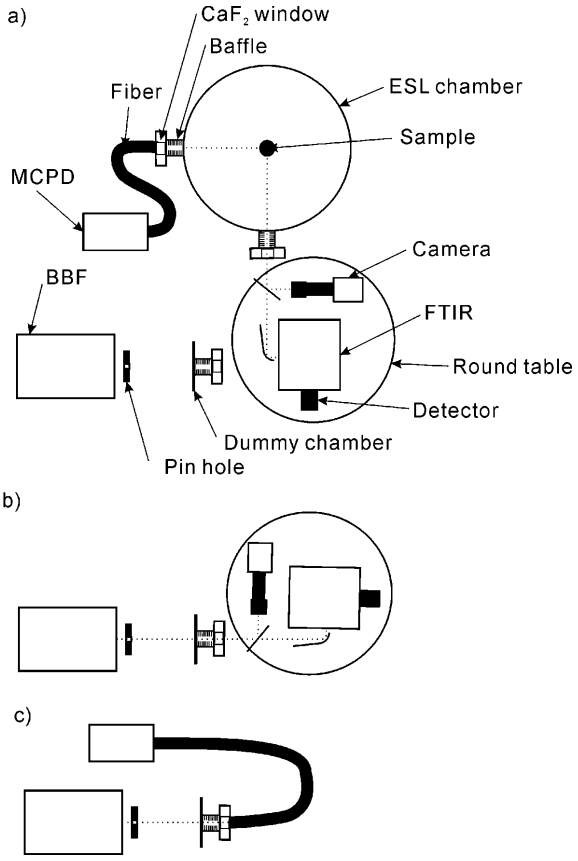


**Fig. 1** Spectral emissivity measurement system combined with an electrostatic levitator; a) setup configuration during levitation experiment, b) calibration of the FTIR, and c) calibration of the MCPD.

sources. It was decided to place the FTIR on a round table, so that the FTIR can observe the light source (levitated sample or blackbody) without any mirrors. A camera with a telephoto lens was placed along the optical path of the FTIR to observe the sample position and to ensure that the optical alignment between the sample and the detector was maintained. Once the sample position was confirmed, the beam splitter in front of the camera was removed to maximize the light intensity to the FTIR. As for the MCPD, a glass fiber was used to introduce the light to the spectrometer.

Baffles were inserted in the chamber to eliminate the internal reflection within the tubes holding the optical windows. $CaF_2$ windows were used because of their good transmission characteristics over the observed wavelength range.

The blackbody furnace was equipped with a simulated chamber wall with a tubular port and an observation window. A pinhole was set in front of the blackbody to simulate a levitated sample. The geometrical arrangement of the simulated sample, the chamber wall, the tubular port, and the window is identical to that of the ESL. Furthermore, the blackbody furnace was set so that the distance from the pinhole to the FTIR was the same as that from levitated sample in the ESL to the FTIR.

### 2.3 Measurement Procedure

For these experiments, ~2 mm diameter spheroid samples were prepared by arc-melting pieces of metal wires of 99.9 wt% purity. Before the levitation experiment, the FTIR and the MCPD were checked with the BBF. Then, both instruments were set to face the electrostatic levitation chamber. Once a sample was levitated in the chamber, it was heated by the $CO_2$ lasers and fully melted. Then, all $CO_2$ lasers were turned off to let the sample cool by radiation. A typical cooling curve (sample temperature vs time) is shown in **Fig. 2**. Since there was no crucible around the sample, it could reach undercooled temperatures. After the recalescence (release of latent heat at solidification from undercooled phase), the sample temperature exhibited a plateau which corresponds to its melting temperature (point c to d in **Fig. 2**). Following this, the power of the $CO_2$ lasers was adjusted so that the sample temperature matched that of the temperature plateau (melting temperature) and maintained for a few minutes, during which time measurements of the light intensity from the sample were made with the FTIR and the MCPD. The sample position was monitored with the telephoto camera coupled to the FTIR and kept at a fixed position. Throughout the experiment, the magnified sample image was recorded for later analysis.

Three detectors were used with the FTIR over a wide spectral range: an InGaAs detector (Newport 80020) (1.2 to 1.5 μm), an extended InGaAs detector (Newport 80014) (2.0 to 2.5 μm), and a HgZnCdTe detector (Newport 77258) (3.1 to 5.5 μm). Since only one detector could be equipped with the FTIR, experiments had to be conducted three times. As for the MCPD, the measurement range (700 to 1000 nm) was selected to avoid the detrimental effects of other light sources used in the system, in particular the position sensing lasers (532 nm and 645 nm) and the UV background illumination light (385 nm).

After the experiments, the recorded images were analyzed to get the sample radius. Also, the FTIR and the MCPD were faced to the BBF for calibration (**Figs. 1b** and **c**). The diameters of pinholes could be varied from 1.0 to 2.5 mm with 0.1 mm intervals. Since these spectrometers were sensitive to the size of the radiation source, two pinholes whose diameters were close to that of the sample were used for the calibration. These pinholes were set one by one and the radiation intensities passing through them were measured. The temperatures of the BBF were changed from 1273 K to 1773 K with 100 K intervals to get the intensity as a function of temperature.

The converting functions from the spectrometer signals ($V_S$) to the radiation intensities were calculated using the calibration data with the BBF ($V_B$). Preliminary experiments proved that the spectrometer signal was proportional to the square of the sample or pinhole radii. Two calibration data with different pinholes were interpolated to make the converting functions for the actual sample size. Then, the measured signals from the detectors obtained during the levitation experiment were converted to the radiation intensities of the sample ($I_S$).

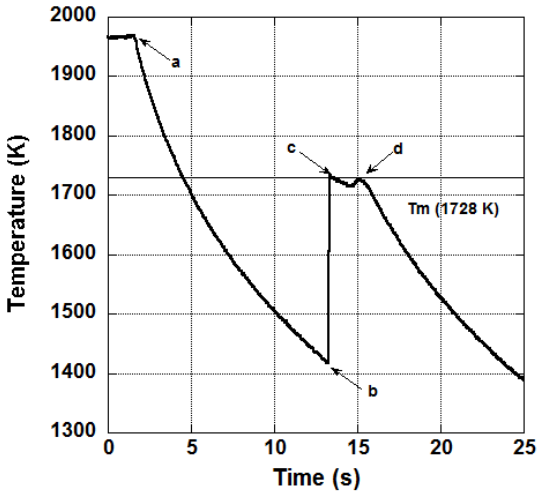


**Fig. 2** Typical cooling curve of molten nickel.

The emissivity is the ratio of energy radiated by a particular material to the energy radiated by a blackbody at the same temperature[15]. The radiation intensity from a blackbody $I_B$ depends on wavelength $\lambda$ and temperature $T$ whereas $I_S$ depends on $\lambda$, $T$, and on the direction of the radiation. The directional spectral emissivity is defined as[15]:

$$\varepsilon(\lambda,\theta,T)=\frac{I_s(\lambda,\theta,T)}{I_B(\lambda,T)} \tag{1}$$

where $\theta$ is the polar angle measured from the normal to the surface of a sample. The directional emissivity with $\theta$ = 0 is called the normal spectral emissivity, which is commonly measured with a variety of methods.

The radiation intensity from a blackbody $I_B$ is given by Planck's law of radiation as follows:

$$I_B=\frac{2C_1}{\lambda^5}\cdot\frac{1}{\exp(C_2/\lambda T)-1} \tag{2}$$

where $C_1$ and $C_2$ are Planck's first and second constants, being respectively 5.96 x $10^{-17}$ W·m$^2$·sr$^{-1}$ and 1.44 x $10^{-2}$ m·K.

Integration of equation (1) over all directions gives the hemispherical spectral emissivity $\varepsilon(\lambda)$ [15]. A merit of ESL is that the levitated molten sample is spherical. When the shape of the emission source is spherical, the radiation becomes isotropic. Therefore, the measured spectral emissivity from the spherical sample is homogeneous in any direction, which means that the measured emissivity with ESL is equal to the hemispherical spectral emissivity.

The total hemispherical emissivity $\varepsilon_T$ can be calculated by integrating the hemispherical spectral emissivity over all wavelengths:

$$\varepsilon_T = \frac{\int \varepsilon(\lambda) I_B(\lambda,T)\,d\lambda}{\int I_B(\lambda,T)\,d\lambda} \approx \frac{\int_{\lambda_1}^{\lambda_2} \varepsilon(\lambda) I_B(\lambda,T)\,d\lambda}{\int_{\lambda_1}^{\lambda_2} I_B(\lambda,T)\,d\lambda} = \frac{\int_{\lambda_1}^{\lambda_2} I_S(\lambda,T)\,d\lambda}{\int_{\lambda_1}^{\lambda_2} I_B(\lambda,T)\,d\lambda} \tag{3}$$

In this research, $\lambda_1$ and $\lambda_2$ are 0.7 μm and 5.5 μm, respectively, and T is the melting temperature.

Once $\varepsilon_T$ is obtained, $C_p$ is calculated from the cooling curve. Since a heated sample cooled purely via radiation in the high vacuum environment of the electrostatic levitator, the energy equation describing the cooling process is given by [7]:

$$\frac{m}{M} c_p \frac{dT}{dt} = -\varepsilon_T A \sigma_{SB} \left(T^4 - T_a^4\right) \tag{4}$$

where $m$ is the sample mass, $M$ is the atomic weight, $T_a$ and $T$ are respectively the ambient and sample temperatures, $A$ is the surface area of the sample, and $\sigma_{SB}$ is the Stefan-Boltzmann constant.

## 3. Experimental Results

### 3.1 Emissivity

**Figure 3** shows the measured radiation intensity of the molten nickel at its melting temperature as a function of wavelength. Radiation intensity of the blackbody calculated by eq. (2) is also plotted in the figure. Spectral emissivity $\varepsilon(\lambda)$ can be obtained by dividing the radiation intensity of nickel by that of the blackbody at each wavelength. Spectral emissivity of nickel as a function of wavelength is shown in the **Figs. 4** and **5** together with the literature values. **Figures 6**, **7**, **8** show the $\varepsilon(\lambda)$ of zirconium, rhodium, and niobium, respectively.

All $\varepsilon(\lambda)$ of these metals showed a negative wavelength dependence (**Table 1**). This tendency can be roughly explained by classical Drude model [23]. In the Drude model, the emissivity of opaque materials is expressed using the refractive index $n$ and the extinction coefficient $k$ as

$$\varepsilon = \frac{4n}{(n+1)^2 - k^2} \tag{5}$$

These optical constants are given using the real and imaginary

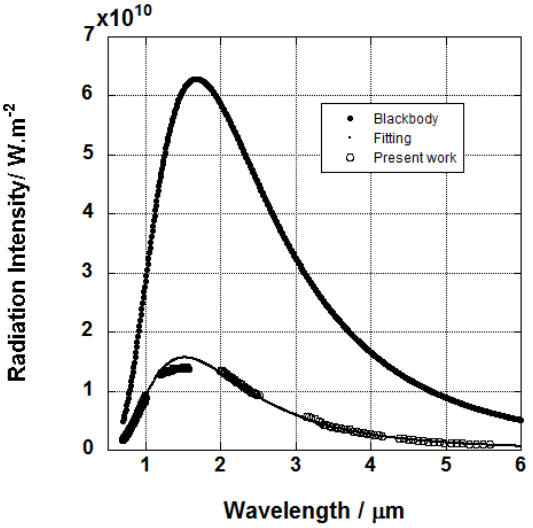


**Fig. 3** Radiation intensity of molten nickel as a function of wavelength.

**Table 1** Wavelength dependence spectral emissivity of $\varepsilon(\lambda)$ of molten metals at their melting temperature.

| | $\varepsilon(\lambda)$ | Ref |
|---|---|---|
| Ni | $\varepsilon(\lambda) = 0.312 \times \lambda^{-0.50}$ | 16 |
| Zr | $\varepsilon(\lambda) = 0.386 - 0.246 \times \log(\lambda)$ | 26 |
| Rh | $\varepsilon(\lambda) = 0.28 \times \lambda^{-0.30}$ | 16 |
| Nb | $\varepsilon(\lambda) = 0.3899 - 0.0691\lambda + 0.005048\lambda^2$ | 34 |

parts $\varepsilon_1(\omega)$ and $\varepsilon_2(\omega)$ of the dielectric function as

$$\varepsilon_1(\omega) = n^2 - k^2 = 1 - \frac{\omega_p{}^2 \tau^2}{1 + \omega^2 \tau^2} \tag{6}$$

and

$$\varepsilon_2(\omega) = 2nk = \frac{\omega_p{}^2 \tau}{\omega(1 + \omega^2 \tau^2)} \tag{7}$$

where $\omega$ denotes the angular frequency of the electric field, $\tau$ represents the relaxation time, and $\omega_p$ is the plasma frequency. $\omega_p$ and $\tau$ can be calculated using the following equations:

$$\omega_p{}^2 = \frac{N \cdot e^2}{m \varepsilon_0} \tag{8}$$

and

$$\frac{1}{\rho_{el}} = \frac{N e^2 \tau}{m} \tag{9}$$

where $N$, $m$, $e$, $\varepsilon_0$, and $\rho_{el}$ are the number of free electrons per unit volume, the effective mass of the electron, the charge of the electron, the permittivity of the vacuum, and the electrical resistivity, respectively. Parameters used for the calculation were listed in **Table 2**, and estimated emissivity values by the Drude model are plotted in **Figs. 4** to **8**.

Drude model can produce the negative wavelength dependence of $\varepsilon$, but quantative agreements are poor. It is well known that Drude model (the nealy free electron model) may not adequately describe the behavior of transition metals because the $d$ electron bands cross the Fermi surface.[24] A new theoretical model is needed to reproduce the wavelength dependence of emissivity more quantitatively.

The value of the total hemispherical emissivity ($\varepsilon_T$) for each metal was calculated with eq. (3). In order to fulfill the gap between detectors, the fitting equations shown in **Table 1** was used. The obtained $\varepsilon_T$ were shown in **Table 3** with the literature values.

### 3.2 Heat capacity

Finally, the $C_p$ of each metal at its melting temperature was calculated using eq. (4), the cooling curve data, and the obtained $\varepsilon_T$. The measured $C_p$ values and the literature values are listed in **Table 4**. Generally, our measured values agreed very well with the literature values, indicating that our measurements were adequate.

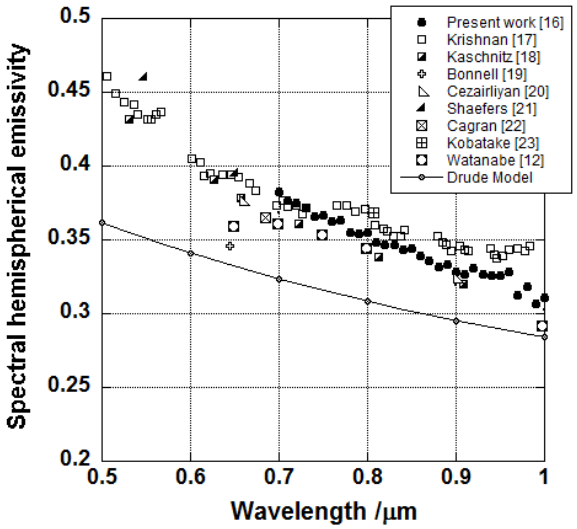


**Fig. 4** Spectral hemispherical emissivity of molten nickel at its melting temperature over the 0.5 to 1 μm range.

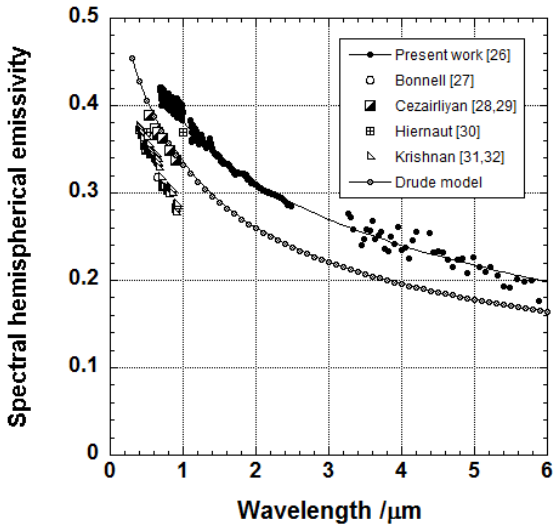


**Fig. 6** Spectral hemispherical emissivity of molten zirconium at its melting temperature over the 1 to 6 μm range.

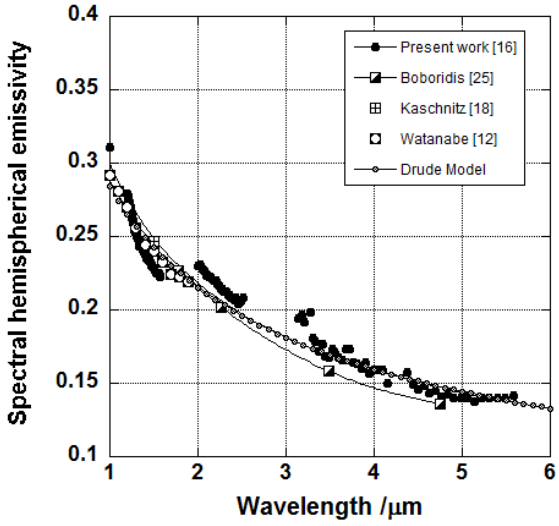


**Fig. 5** Spectral hemispherical emissivity of molten nickel at its melting temperature over the 1 to 6 μm range.

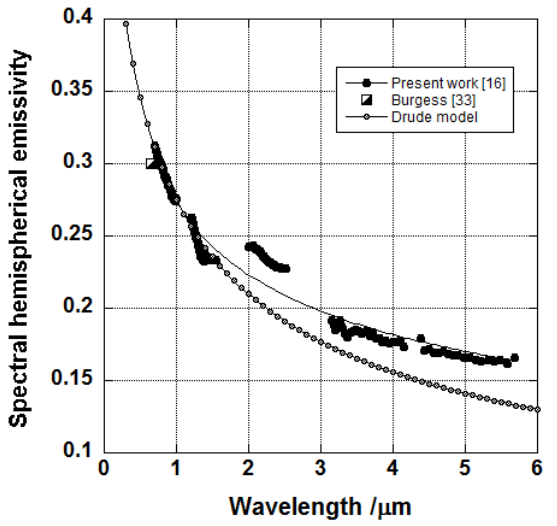


**Fig. 7** Spectral hemispherical emissivity of molten rhodium at its melting temperature over the 1 to 6 μm range.

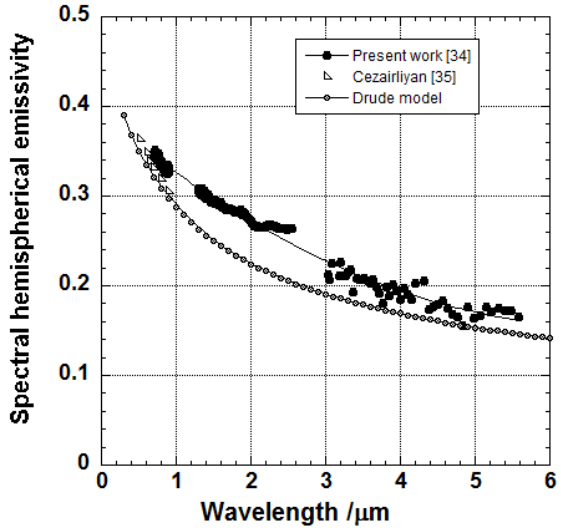


**Fig. 8** Spectral hemispherical emissivity of molten rhodium at its melting temperature over the 1 to 6 μm range.

$C_p$ of liquid refractory metals has been measured mainly by two methods, levitation calorimetry and pulse heating. In the levitation calorimetry, samples were electromagnetically levitated and melted, then their enthalpy were measured by drop calorimetry. The $C_p$ could be obtained from the temperature – enthalpy plot. This method needs many samples to be levitated, molten and dropped to get a temperature dependence of enthalpy. This time-consuming way of doing things probably explains why the values reported by this method are limited. The pulse heating method also measures the enthalpy as a function of temperature to get $C_p$. The experimental procedure is simple (only one sample is needed) but the measurement must be done in a sub-second time of frame. The reported values in 1970s show a large scatter, maybe due to the technical limitations for rapid measurements at that time. As fast measurement techniques have been developed, the reported values by the pulse heating method began to converge towards those obtained by levitation calorimetry. Compared with these two methods, our new method by ESL uses medium number of samples and medium measurement time.

## 4. Conclusions

The spectral hemispherical emissivity of molten metals over wide wavelength range was measured by spectrometers combined with an ESL. The $\varepsilon_T$ and the $C_p$ that were calculated from the data agreed very well with the literature data, which proved the validity of the measurement scheme. Moreover, this shows that the ESL has the capability to measure the $C_p$ and $\varepsilon_T$ without borrowing any literature data, which enables the measurements of these properties for refractory metals such as tungsten, tantalum, or rhenium in their molten state.

**Table 2** Parameters used for Drude model calcuration.

| Parameters | | |
|---|---|---|
| Temperature /K | Ni | 1728 |
| | Zr | 2128 |
| | Rh | 2236 |
| | Nb | 2742 |
| Density $\rho$ /kg· m$^{-3}$ | Ni | 7.85 x 10$^3$ |
| | Zr | 6.21×10$^3$ |
| | Rh | 1.08 x 10$^4$ |
| | Nb | 7.73×10$^3$ |
| Electrical resistivity $\rho_{el}$ /Ω·m | Ni | 9.3 x 10$^{-7}$ |
| | Zr | 1.38×10$^{-6}$ |
| | Rh | 8.9 x 10$^{-7}$ |
| | Nb | 1.09×10$^{-6}$ |
| Number of electrons $N$ /m$^{-3}$ | Ni | 6.44 x 10$^{29}$ |
| | Zr | 1.64 x 10$^{29}$ |
| | Rh | 5.07 x 10$^{29}$ |
| | Nb | 2.58 x 10$^{29}$ |
| Atomic weight /kg·mol$^{-1}$ | Ni | 5.87 x 10$^{-2}$ |
| | Zr | 9.12×10$^{-2}$ |
| | Rh | 1.03 x 10$^{-1}$ |
| | Nb | 9.29×10$^{-2}$ |
| $m$ /kg | | 9.019 x 10$^{-31}$ |
| $e$ /C | | 1.602 x 10$^{-19}$ |
| $\varepsilon_0$ /F·m$^{-1}$ | | 8.854 x 10$^{-12}$ |
| Avogadro's constant | | 6.022 x 10$^{23}$ |

**Table 3** Total hemispherical emissivity of molten metals at their melting temperatures.

| | $\varepsilon_T$ | Reference | Remarks |
|---|---|---|---|
| Ni | 0.21 | Present study[16)] | ESL |
| Zr | 0.32 | Present study[26)] | ESL |
| | 0.29 | Rulison [8)] | ESL (borrowing heat of fusion 14.652 x 10$^3$ J/mol) |
| | 0.308 | Sung[9)] | ESL (borrowing $C_p$ from JANAF[36)]) |
| Rh | 0.23 | Present study[16)] | ESL |
| Nb | 0.29 | Present study[34)] | ESL |
| | 0.25 | Paradis[37)] | ESL (borrowing Cp 40.6 Jmol$^{-1}$K$^{-1}$) |
| | 0.25 | Sung[38)] | ESL (borrowing Cp 41.78 Jmol$^{-1}$K$^{-1}$) |

## Acknowledgment

This work was partially supported by a Grant-in-Aid for Science Research (B) No. 18360108 from the Japan Society for the Promotion of Science.

**Table 4** Constant pressure heat capacity of metals at their melting temperatures.

| | $C_p$(J·mol$^{-1}$·K$^{-1}$) | Reference | Remarks |
|---|---|---|---|
| Ni | 39.9 | Present work [16] | ESL |
| | 38.49 | Kubaschewski [40] | |
| | 40.819 | Pottlacher[41] | Pulse heating |
| | 36.2 | Ishikawa[42] | ESL |
| | 43.1 | Barin[43] | Calculated |
| | 38.911 | JANAF [36] | |
| Zr | 40.9±1.6 | Present work[26] | ESL |
| | 40.7 ± 0.7 | Bonnell[27] | Drop calorimetry with EML |
| | 40.8 ±0.9 | Rulison [8] | ESL (borrowing heat of fusion 14.652 x $10^3$ J/mol) |
| | 39.72 | Paradis[44] | ESL (borrowing $\varepsilon_T$ from Bonnell[26]) |
| | 41.84 | Sung[9] | ESL (borrowing $C_p$ from JANAF[35]) |
| | 41.84 | JANAF[36] | |
| | 38.5 | Korobenko[45] | Pulse heating |
| | 32.8-44.7 | Kats[45] | Levitation calorimetry |
| | 42.4 | Fink[45] | |
| | 45.274 | Brunner[46] | Pulse heating |
| | 33.47 | Barin[43] | Calculated |
| Rh | 41.8 | Present work [16] | ESL |
| | 46.102 | Hüpf [47] | Pulse heating |
| | 32.2 | Paradis [48] | ESL ($\varepsilon_T$ = 0.18) |
| | 41.8 | Jaeger [49] | |
| | 41.84 | Barin [43] | Calculated |
| Nb | 41.9 | Present study [34] | ESL |
| | 43.294 | Pottlacher [41] | Pulse-heating measurements |
| | 41.78 | Kubaschewski [39] | |
| | 33.472 | JANAF [36] | |
| | 40.60 | Bonnel [27] | Drop calorimetry with EML |

## References


1) T. Hibiya and I.Egry: Meas. Sci. Technol., **16** (2005) 317.
2) W.–K. Rhim, S.K. Chung, D. Barber, K.F. Man, G. Gutt, A. Rulison and R.E. Spjut: Rev. Sci. Instrum., **64** (1993) 2961.
3) S.K. Chung, D.B. Thiessen and W-K. Rhim: Rev. Sci. Instrum., **67** (1996) 3175.
4) W.-K. Rhim, K. Ohsaka, P.-F. Paradis and R.E. Spjut: Rev. Sci. Instrum, **70** (1999) 2796.
5) R.K. Wunderlich, Ch. Ettl and H.-J. Fecht: Int. J. Thermophys., **22** (2001) 579.
6) H. Kobatake, H. Fukuyama, T. Tsukada and S. Awaji: Meas. Sci. Technol., **21** (2010) 025901.
7) A.J. Rulison and W.-K. Rhim: Rev. Sci. Instrum., **65** (1994) 695.
8) A.J. Rulison and W.K. Rhim: Met. and Mat. Trans, **26B** (1995) 503.
9) Y.S. Sung, H. Takeya and K. Togano: Jpn. J. Appl. Phys., **41** (2002) L895.
10) T. Ishikawa, P.–F. Paradis, T. Itami and S. Yoda: Meas. Sci. Technol., **16** (2005) 443.
11) W.-K. Rhim and T. Ishikawa: Rev. Sci. Instrum., **69** (1998) 3628.
12) H. Watanabe, M. Susa, H. Fukuyama and K. Nagata: Int. J. Thermophys., **24** (2003) 473.
13) H. Kawamura, H. Fukuyama, M. Watanabe and T. Hibiya: Meas. Sci. Technol., **16** (2005) 386.
14) R.W. Hyers and J.R. Rogers: High Temperature Materials and Processes, **27** (2008) 461.
15) M. Susa and R.K. Endo: High temperature measurements of materials, ed. H. Fukuyama and Y. Waseda, Springer, Berlin Heiderberg, **6** (2009) 112.
16) T. Ishikawa, J.T. Okada, P.-F. Paradis and Y. Watanabe: J. Chem. Thermodynamics, **103** (2016) 107.
17) S. Krishnan, K.J. Yugawa and P.C. Nordine: Phys. Rev., **B55** (1997) 8201.
18) E. Kaschnitz, J.L. McClure and A. Cezairliyan: Int. J. Thermophys., **19** (1998) 1637.
19) D.W. Bonnell, J.A. Treverton, A.J. Valerga and J.L. Margrave: Temperature, ed. H.H. Plumb, part 1, ISA, Pittsburgh, **4** (1972) 483.
20) A. Cezairliyan, A.P. Miller, P. Righini and A. Rosso: Temperature, ed. J. F. Schooley, Part 1, AIP, New York, **6** (1992) 377.
21) K. Shaefers, M. Rösner-Kuhn and M.G. Frohberg: Int. J. Thermophys., **16** (1995) 997.
22) C. Cagran, B. Wilthan and G. Pottlacher: High Temp.- High Press., **35**/**36** (2003/2007) 667.
23) H. Kobatake, H. Khosroabadi and H. Fukuyama: Met. & Mat. Trans., **43A** (2012) 2446.
24) K.J. Daun: Met. & Mat. Trans., **47A** (2016) 3300.
25) K. Boboridis, A. Seifter, A.W. Obst and D. Basak: Int. J. Thermophys., **28** (2007) 683.
26) T. Ishikawa, Y. Ito, J.T. Okada, P.–F. Paradis, Y. Watanabe and T. Masaki: Meas. Sci. Technol., **23** (2012) 125602.
27) D.W. Bonnell: Ph.D thesis, Rice University (1972)
28) A. Cezairliyan and F. Righini: Journal Research of the National Bureau of Standard-A Physics and Chemistry, **78A** (1974) 509.

29) A. Cezairliyan, J.L. McClure and A.P. Miller: Int. J. Thermophys., **15** (1994) 993.
30) J.P. Hiernaut, F. Sakuma and C. Ronchi: High Temp. High Press., **21** (1989) 139.
31) S. Krishnan, J.K.R. Weber, C.D. Anderson, P.C. Nordine and R.I. Sheldon: J. Nuc. Mater., **203** (1993) 112.
32) S. Krishnan, C.D. Anderson and P.C. Nordine: 1994 Phys. Rev., **B49** (1994) 3161.
33) G. Burgess and R. Waltenberg: National Bur. Stds. Bull., **11** (1915) 591.
34) K. Sakata, Y. Watanabe, J.T. Okada, M.V. Kumar, P.–F. Paradis and T. Ishikawa: J. Chem. Thermodynamics, **91** (2015) 116.
35) A. Cezairliyan and A.P. Miller: Int. J. Thermophys., **13** (1992) 39.
36) J. of Phys. & Chem. Ref. Data Vol.14 Suppl. 1, JANAF Thermophysical Tables, ed. D.R. Lide Jr., 3rd ed., Part II (1849), American Chem. Society & American Inst. of Phys., New York (1985).
37) P.-F. Paradis, T. Ishikawa and S. Yoda: J. of Materials Science, **36** (2001) 5125.
38) Y.S. Sung: J. Appl. Phys., **92** (2002) 6531.
39) O. Kubaschewski, C.B. Alcock and P.J. Spencer: Materials Thermochemistry, 6th ed., Pergamon, New-York (1993).
40) O. Kubashewski and C.B. Alcock: Metallurgical thermochemistry 5th ed, 14, Butterworth-Heinemann (1992).
41) G. Pottlacher: High Temperature Thermophysical Properties of 22 Pure Metals, 62, Edition Keiper, Austria (2010).
42) T. Ishikawa, P.-F. Paradis and Y. Saita: J. Japan Inst. Metals, **68** (2004) 781. (in Japanese)
43) I. Barin and O. Knacke: Thermophysical properties of inorganic substances, Springer-Verlag (1973).
44) P.-F. Paradis and W.-K. Rhim: J. Mater. Res., **14** (1999) 3713.
45) V.N. Korobenko and A.I. Savvatimskii: High Temperature, **39** (2001) 659.
46) C. Brunner, C. Cagran, A. Seifter and G. Pottlacher: Temperature, American Institute of Physics, **7** (2003) 771.
47) T. Hüpf, C. Cagran, B. Wilthan and G. Pottlacher: J. Phys., Condens. Matter., **21** (2009) 125701.
48) P.-F. Paradis, T. Ishikawa and S. Yoda: Int. J. Thermophys., **24** (2003) 1121.
49) F.M. Jaeger and E. Rosenbohm: Rec. Trav. Chim., **51** (1932) 1.